Comprehensive study of the metal-insulator transition in pulsed laser deposited epitaxial VO$_2$ thin films

Deyi Fu,[1,2,a)] Kai Liu,[1,3,a)] Tao Tao,[2] Kelvin Lo,[1] Chun Cheng,[1] Bin Liu,[2] Rong Zhang,[2] Hans A. Bechtel,[4] and Junqiao Wu[1,3,b)]

[1]*Department of Materials Science and Engineering, University of California, Berkeley, California 94720, USA*
[2]*Jiangsu Provincial Key Laboratory of Advanced Photonic and Electronic Materials, School of Electronic Science and Engineering, Nanjing University, Nanjing, Jiangsu 210093, China*
[3]*Materials Sciences Division, Lawrence Berkeley National Laboratory, Berkeley, California 94720, USA*
[4]*Advanced Light Source, Lawrence Berkeley National Laboratory, Berkeley, California 94720, USA*

In this paper, we present a comprehensive, correlative study of the structural, transport, optical and thermoelectric properties of high-quality VO$_2$ thin films across its metal-insulator phase transition. Detailed x-ray diffraction study shows that it's textured polycrystalline along $[010]_{M1}$, with in-plane lattice orienting along three equivalent crystallographic directions. Across the metal-insulator transition, the conductivity increases by more than 3 orders of magnitude with a value of 3.8×10^3 S/cm in the metallic phase. This increase is almost entirely accounted for by a change in electron density, while the electron mobility changes only slightly between the two phases, yet shows strong domain boundary scattering when the two phases coexist. Electron effective mass was determined to be $\sim 65 m_0$ in the insulating phase. From the optical and infrared reflection spectra in the metallic phase, we obtained the plasma edge of VO$_2$, from which the electron effective mass was determined to be $\sim 23 m_0$. The bandgap of VO$_2$ was determined from optical absorption to be 0.70 ± 0.05 eV at room temperature and rapidly shrinks before the phase transition occurs. In the temperature range where metallic and insulating phases coexist, the Seebeck coefficient was found to be significantly lower than that predicted by a linear combination of volumetric contributions from the insulating and metallic domains, indicating abnormal thermoelectric effect at the metal/insulator domain walls in such two-dimensional domain structure. © *2013 American Institute of Physics.* [http://dx.doi.org/10.1063/1.4788804]

I. INTRODUCTION

Vanadium oxides exhibiting metal-insulator transition (MIT) at various temperatures are of great interest in materials science for both fundamental understanding of correlated electron physics and potential device applications. Among them, vanadium dioxide (VO$_2$) has been studied most intensively owing mostly to its near-room-temperature phase transition as well as its high phase stability.[1] It undergoes a first-order MIT around 68 °C from a high-temperature metallic (M) phase to a low-temperature insulating (I) phase, which is accompanied by a structural phase transition from a high-temperature tetragonal (Rutile, R) structure to a low-temperature monoclinic (M1) structure.[2–6] Both theoretical and experimental efforts have been devoted to understanding and exploiting the mechanism of MIT since the early work of Morin decades ago.[7] However, due to the complex phase diagram of VO$_{2-\delta}$ with different stoichiometries, as well as complications arising from coexisting metal/insulator domains across the MIT, the synthesis and characterization of VO$_2$ have never been easy. Thanks to rapid advances in growth of thin-film oxides in recent years such as molecular beam epitaxy,[8] chemical vapor deposition,[9] sol-gel deriving,[10] sputtering,[11] and pulsed laser deposition,[12] the study of VO$_2$ is reviving, with growing emphasis on exploring its device applications. Applications such as thermo/electrochromics,[13] Mott transistors,[14] strain sensors,[15] and thermal actuators[16] have been proposed or realized based on the MIT of VO$_2$.

However, a systematic, comprehensive study of the physical properties of these high-quality VO$_2$ specimens across the MIT has been lacking; for example, electrical transport properties were measured without optical and infrared characterization of the same sample[17] and vice versa.[18] As a result, correlations across different aspects of the MIT are yet to be identified and cross-checked, which could reveal some intrinsic materials properties out of merely sample-specific effects, or answer outstanding questions on VO$_2$. In this work, we present a comprehensive study of high-quality VO$_2$ thin films grown by pulsed laser deposition, fully characterizing their structural, electrical transport, optical (including infrared), and thermoelectric properties altogether. These include: (1) The growth direction of epitaxial VO$_2$ thin films on sapphire is identified to be $[010]_{M1}$ instead of $[001]_{M1}$, a controversy from previous reports. Identification of the film texturing direction is important to simulation of energetics of the VO$_2$ phase transition strain,[19] as well as the very recent effort of using VO$_2$ as an active material for MEMS actuation;[20] (2) An unusually strong electron scattering by M-I domain boundaries is revealed from the electron mobility drop during the inhomogeneous MIT of VO$_2$. Such effect disappear when the

a)Deyi Fu and Kai Liu contributed equally to this work.
b)Author to whom correspondence should be addressed. Electronic mail: wuj@berkeley.edu.

film is in pure M or I phase, therefore must originate from scattering of electrons at the interface between M and I phases, and differ from the ordinary grain boundary scattering. It may need to be included for properly analyzing free charge dynamics in optical studies of VO_2 films in the M-I phase co-existing regime;[18] (3) From the plasma edge on the infrared reflectance, we determine the electron effective mass in the M-phase, which is cross-checked by independent Seebeck measurement; (4) By combining Hall and Seebeck measurements, we conclude that lattice (acoustic phonon) scattering of conductive electrons in the M-phase is negligible; (5) The Fermi level in the I-phase is determined by temperature-dependent Seebeck measurement, which is then combined with the temperature-dependent Hall data to evaluate the electron effective mass of the I-phase; (6) Combining Hall mobility data and Seebeck results highlights the important unusual thermoelectric contribution of M-I domain walls during the inhomogeneous MIT of the thin film system, which proves that this domain wall effect is not limited to 1D VO_2 nanobeams;[21] (7) The bandgap of I-phase VO_2 is determined, and its temperature dependence is found to be an order of magnitude stronger than that of non-correlated, traditional semiconductors. These results are expected to help further understanding of this correlated electron oxide, as well as its future device applications in electronics and electro-optics.

II. EXPERIMENTAL

The VO_2 thin films used in this study were grown on *c*-plane sapphire (i.e., (0001)-Al_2O_3) substrate by pulsed laser deposition. A KrF excimer laser ($\lambda = 248$ nm) was focused onto a target (pressed 99.9% pure VO_2 powder, density ~ 4.0 g/cm^3) with a fluence of ~ 1.3 J/cm^2. The deposition chamber was pumped to $\sim 10^{-6}$ Torr before oxygen gas was introduced into the chamber. The deposition was performed in oxygen ambient of 10 mTorr with substrate temperature maintained at $530\,^\circ$C for 2.5 h. After the deposition, the samples were cooled down at a rate of $10\,^\circ$C/min to room temperature at the deposition oxygen pressure. The thickness of the as-grown film was determined to be ~ 250 nm by cross-sectional scanning electron microscopy and atomic force microscopy (AFM).

The crystallinity of the films at room temperature (M1-structure) was first identified by high resolution x-ray diffraction, which was performed using a triple-axis diffractometer equipped with a four-crystal Ge (220) monochromator and a three reflection Ge (220) analyzer in a PANalytical X'Pert Pro MRD system. The Cu Kα line ($\lambda = 0.154$ nm) radiated from a 2.2 kW ceramic tube with resolution limit of about 12 arc sec was used as the x-ray source.

Transport properties across the MIT, such as temperature dependence of the electrical resistivity/conductivity, carrier density and Hall mobility, were measured based on van der Pauw geometry using an Ecopia HMS-3000 Hall measurement system. The sample temperature was controlled by a Lake Shore 325 temperature controller with high temperature stability and was calibrated with a thin type-K thermocouple.

To investigate optical properties across the MIT, both reflection and transmission spectra were taken from ultraviolet to the infrared wavelength range. The mid-infrared spectra between 1600 cm^{-1} and 7000 cm^{-1} were measured using a Fourier-transform infrared spectrometer (Thermo Nicolet Nexus870) combined with a confocal microscope (Nicolet ContinuumXL) using a $32\times$ Schwarzschild objective (numerical aperture:0.65), and the signal was collected with a liquid-nitrogen-cooled mercury cadmium telluride (MCT-A) detector (as shown elsewhere[22]). The ultraviolet-visible-near-infrared spectra between 320 nm and 2600 nm were measured using a PerkinElmer LAMBDA 750 UV/Vis/NIR spectrophotometer, where the signal below 890 nm was collected by a photomultiplier tube and that above 890 nm was collected by a PbS detector.

A rectangular sample ($\sim$10 mm $\times$ 5 mm) with Ohmic contacts (15 nm Cr/200 nm Au) on the two ends of the stripe was prepared for the Seebeck measurement. The Seebeck measurement was carried out by suspending the sample between two temperature controlled copper blocks, which were enclosed inside a small vacuum chamber providing pressures as low as 9×10^{-7} Torr. High temperatures were produced by passing current through resistive heaters in each sample block. The temperature at each end of the sample was monitored by affixing type-T thermocouples to either end using small pieces of indium foil to ensure good thermal contact to the sample.

III. RESULTS AND DISCUSSION

A. Structural properties

Figure 1(a) shows the XRD $2\theta/\omega$ scan spectra of the as-grown VO_2 thin film at room temperature. The well-resolved sharp peaks at 41.94° and 90.98° correspond to diffraction peaks from the *c*-plane of the substrate, namely sapphire(0006) and sapphire(00012), respectively. However, the origin of the peak located around 40.02° and its secondary peak at 85.97° have been controversial, and they have been indexed as either $(020)_{M1}/(040)_{M1}$ peaks, or $(002)_{M1}/(004)_{M1}$ peaks, of VO_2 by different groups.[12,23–26] The discrepancy originates from the fact that $(010)_{M1}$ and $(001)_{M1}$ planes of VO_2 have almost the same lattice spacing, therefore nearly the same Bragg diffraction angle, which makes them undistinguishable by using only $2\theta/\omega$ scan. In order to solve the problem and also explore the in-plane texturing of the film, off-axis φ scan of VO_2 $(110)_{M1}$ planes were performed because they have significantly different inclination angles to the VO_2 $(010)_{M1}$ and $(001)_{M1}$ planes. As shown in Fig. 1(b), only the diffraction peaks from the φ scan patterns corresponding to the $[010]_{M1}$ growth direction ($\Psi = 43.1^\circ$, $2\theta = 26.86^\circ$) were found, which verifies high-quality crystalline VO_2 with its $(010)_{M1}$ plane (rather than $(001)_{M1}$ plane) parallel to the substrate. The high quality of the film is evident from the relative small full width at half-maximum (FWHM $\sim 0.15^\circ$) of the rocking curve of the $(020)_{M1}$ diffraction peak as shown in the inset of Fig. 1(a). We note that the VO_2 peaks and their rocking curves slightly deviate from an ideal Gaussian shape, which is indicative of high residual strain in the thin film due to lattice and thermal mismatches between the VO_2 and the substrate. Furthermore, clear six-fold symmetry of the off-axis φ scan spectra from the
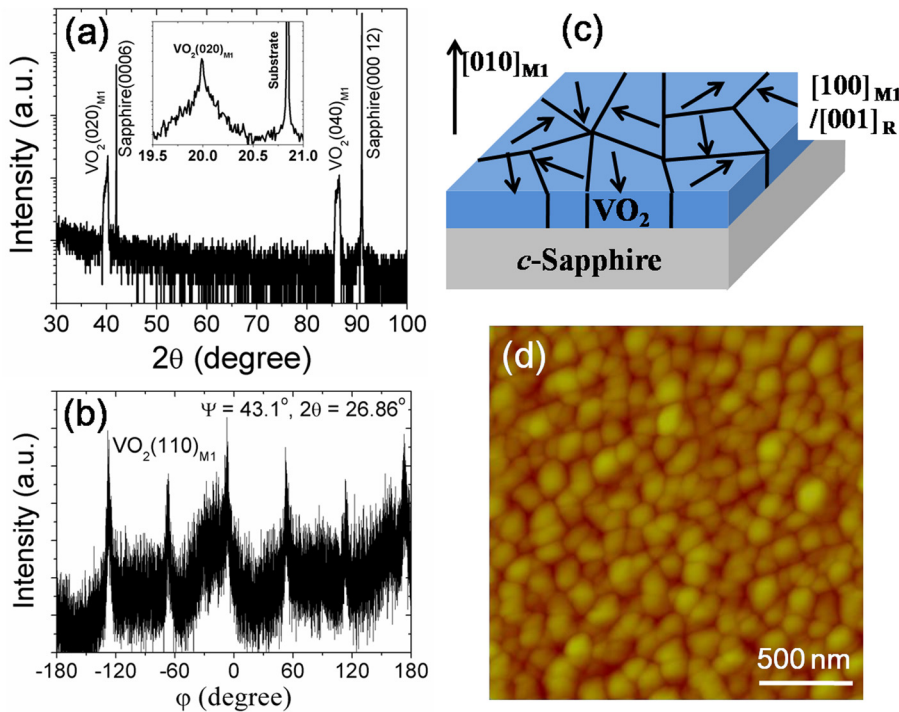
FIG. 1. Structural properties at room temperature. (a) XRD $2\theta/\omega$ scan, (b) φ scan of $(110)_{M1}$ planes corresponding to $[010]_{M1}$ growth direction, (c) schematic of the texturing with different in-plane lattice orientations, and (d) AFM image of the as-grown VO_2 thin film. Inset of (a) shows the rocking curves of both VO_2 $(020)_{M1}$ peak and the substrate peak.

$(110)_{M1}$ planes (Fig. 1(b)) as well as the $(011)_{M1}$ planes (not shown here) implies a highly textured in-plane structure where the in-plane orientations of VO_2 (e.g., $[100]_{M1}$, which is equivalent to $[001]_R$) are rotated by $60°$ about its growth direction (i.e., $[010]_{M1}$-axis or $[100]_R$-axis).[27] Therefore, the VO_2 thin film is $[010]_{M1}$-oriented polycrystalline with in-plane lattice orienting along three equivalent crystallographic directions as sketched in Fig. 1(c), epitaxially registered with the *c*-plane sapphire substrate, with VO_2 $[100]_{M1}$ (or equivalently $[001]_R$) parallel to sapphire $[1000]$, $[0100]$, and $[0010]$ respectively.[28] Figure 1(d) shows an AFM image of the VO_2 thin film grown on *c*-sapphire substrate. Small crystalline grains with size of ~ 120 nm were clearly resolved. The film surface is smooth, with a root mean square roughness of ~ 3 nm.

B. Transport properties

As pointed out in Ref. 17, Hall effect measurements of VO_2 films across its MIT are challenging because of the intrinsically low Hall mobility, the high carrier density that results in low Hall voltage, and the large amount of noise ascribed to the strain present in the sample arising from the discontinuous lattice transformation. The configuration for van der Pauw Hall measurement is depicted in Fig. 2(a), and the sample was mounted on an aluminum tape with a resistive heater embedded underneath. The measurement was done with a slow heating and cooling cycle, and at each temperature point the sample was stabilized for about 3 min, and measured 5 times to check reproducibility. The sign of the Hall voltage indicates that electrons were responsible for the conduction, which is in agreement with previous reports on VO_2 single crystals and nanowires. Since the heating and cooling processes showed consistent results, only the measured data from heating process are presented. As can be seen from Fig. 2(b), the resistivity/conductivity experiences a

change of more than 3 orders of magnitude across the MIT from $60°C$ to $80°C$ and the conductivity is as high as 3.8×10^3 S/cm for the metallic phase. We note that along the temperature axis, the MIT occurs gradually in the thin film as opposed to an abrupt transition in strain-free, single crystalline nano/microwires,[29] which is a manifestation of inhomogeneous MIT in VO_2 thin films due to its poly-crystallinity and strain from substrate clamping.[18] The temperature-dependent carrier density n and mobility μ are shown in Figs. 2(c) and 2(d), respectively. Note that the error bars for these data points are smaller than the size of the symbols in Fig. 2(c). The electron density is $(1.9 \pm 0.2) \times 10^{19}$ in the insulating phase around room temperature and increases by over 3 orders of magnitude across the MIT from $(4.5 \pm 0.5) \times 10^{19}$ cm^{-3} at $60°C$ to $(1.9 \pm 0.5) \times 10^{23}$ cm^{-3} at $80°C$; this change in n almost entirely accounts for the change of resistivity/conductivity shown in Fig. 2(b). These results are consistent with recently reported values found in VO_2 thin films deposited on Si substrate by sputtering method.[17] We note that
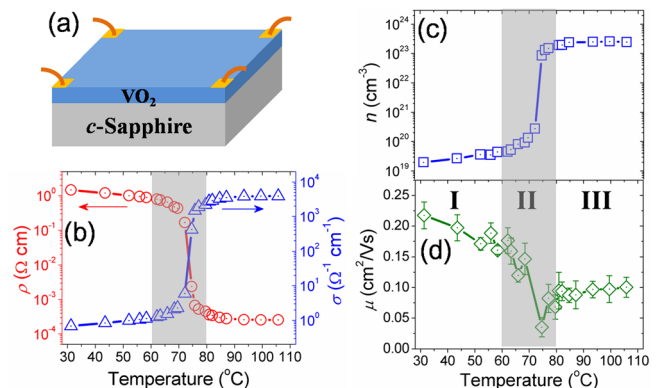

FIG. 2. Transport properties. (a) Schematic of the van der Pauw Hall measurement geometry. (b) Resistivity/conductivity, (c) electron concentration, and (d) electron mobility measured as a function of temperature.

that the measured electron density in the metallic phase corresponds to approximately 7 ± 2 electrons contributed by each vanadium atom since the number density of vanadium atoms in VO$_2$ is about 3×10^{22} cm^{-3}.[2] The observation of more than one conduction electron per vanadium atom has been reported before by different groups[2,17,30] and was explained as two types of carriers co-existing in the system. While the electron density n changes monotonically with temperature, the evolution of mobility μ shows some complexity as seen in Fig. 2(d). The overall mobility in the insulating phase is higher than that in the metallic phase. The whole process can be divided into three regimes: when T < ∼ 60 °C (regime-I), the mobility slightly decreases with increasing temperature; when the temperature further increases and the inhomogeneous MIT and structural transition start to occur (60 °C < T < 80 °C, regime-II), the mobility decreases drastically by a factor of 4, which can be mainly attributed to strong scattering of electrons at the boundaries of metallic and insulating (semiconducting) domains; when the system finally becomes fully metallic (T > ∼ 80 °C, regime-III), the electron mobility partially recovers because the phase boundary scattering effect disappears (even though the structural grain boundaries still exist). We note that the mobility in the metallic phase stays almost a constant upon further heating, suggesting that the mobility there is not governed by acoustic phonon scattering, because phonon scattering would become stronger when temperature rises.

C. Optical and infrared properties

Figure 3 shows the measured optical reflection spectra of the VO$_2$ thin film at selected temperatures during heating. The dashed line distinguishes the spectra measured from two different systems as described in the experimental section. The periodic fringes seen in the insulating-phase spectra ($\leq$65 °C) result from interference between light reflected from the sample top and bottom surfaces (Fabry-Perot oscillation). This interference disappears for the metallic phase due to strong optical absorption by the film. Across the MIT, the reflectivity
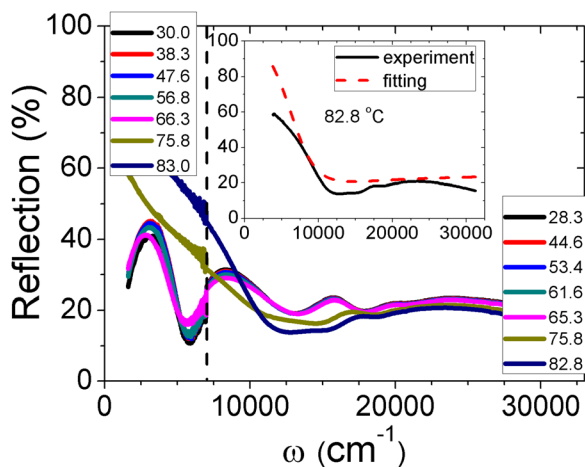
underwent a drastic change, especially in the infrared region (<10 000 cm^{-1}). In the metallic phase (>82 °C), the optical response of the film is dominated by its free carriers and shows high infrared reflectivity. The surface reflection of conductors by free carriers is frequently used to determine the effective mass of free carriers, which can be calculated from the plasma frequency (ω_P), provided that the carrier concentration(n) and the optical dielectric constant (ε_∞) are known,[31] i.e.

$$m^* = \frac{ne^2}{\varepsilon_0 \varepsilon_\infty \omega_P^2},\tag{1}$$

where ε_0 is the vacuum permittivity and e is elementary electron charge. Here, we note that the plasma reflection edge in the insulating-phase is not resolved due to relatively low electron concentration (thus low plasma frequency) and the Fabry-Perot feature. The infrared reflection spectrum for the metallic phase can be fitted using a standard complex dielectric function model that includes finite lifetime broadening,[31] from which ω_P and the damping parameter were determined to be 10 500 cm^{-1} and 15 000 cm^{-1}, respectively, as shown in the inset of Fig. 3. Using the optical dielectric constant $\varepsilon_\infty = 9$ as suggested by Barker *et al.*,[32] we estimated the electron effective mass in the metallic phase to be $\sim$23m_0. This is heavier than previously reported results, which show a range of values between 3.5m_0[30] and 7.1m_0.[33] The higher m^* is mainly due to higher free electron density measured in our films and used in the calculation. This high electron density may also arise from the high residual strain existing in the films.

Optical absorption (α) spectra of the VO$_2$ thin film were obtained by considering the reflection loss, $I_t = I_0(1-R)e^{-\alpha d}$, where d is the film thickness, $R = I_r/I_0$ is the reflection, and I_t/I_0 is defined as transmission T. The value of α converted from measured R and T are shown in Fig. 4(a). A clear onset of absorption at around 0.7 eV can be seen in the insulating phase, which is associated with optical transition across the fundamental bandgap of VO$_2$. Above the threshold energy, the absorption increases rapidly and gradually saturates at around 1.5 eV $\sim$ 2.0 eV, after which the absorption rapidly increases again. The rapid increase beyond $\sim$2.0 eV can be attributed to transition to the conduction band (derived from vanadium 3d-orbitals) from the
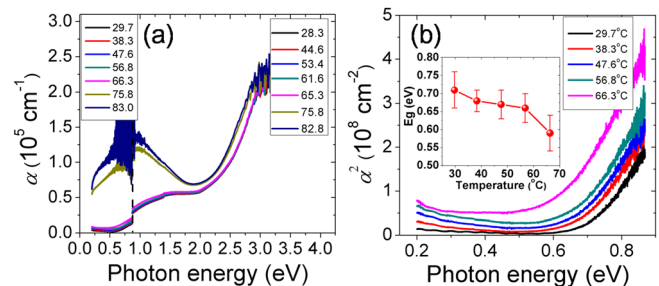

FIG. 3. Reflection spectra of VO$_2$ thin film across a wide spectral range at different temperatures (in units °C). Note that the spectra on the two sides of the vertically dashed line were measured using two different spectroscopy systems. The inset shows the measured and fitted results of the reflection spectrum of VO$_2$ in the high-temperature metallic phase.

FIG. 4. (a) Absorption coefficient of VO$_2$ thin film over a wide spectral range at different temperatures (in units °C). Note that the spectra on the two sides of the vertically dashed line were measured using two different spectroscopy systems. (b) Square of the absorption coefficient of VO$_2$ used to determine the absorption edge of the material. The inset shows the rapid shrink of the absorption edge as a function of temperature.

low-lying oxygen 2p band, which was reported to be $\sim$2 eV below the 3d orbitals.[2] According to the Tauc relation, the absorption coefficient for direct-bandgap material near the band edge can be modeled as[34]

$$\alpha(h\nu) = A\sqrt{h\nu - E_g}, \tag{2}$$

where E_g is the energy gap and A is a constant depending on the material. In Fig. 4(b), we plotted α^2 as a function of photon energy. By fitting the linear section of the absorption spectra and extrapolating to the axis, we determined the bandgap of insulating-phase VO$_2$. When the temperature increases toward the MIT temperature, the effective bandgap gradually decreases, from 0.70 ± 0.05 eV at 30 °C to 0.58 ± 0.05 eV at 66.3 °C. This bandgap narrowing of 0.12 eV from 30 to 66.3 °C (inset of Fig. 4(b)) is an order of magnitude faster than traditional semiconductors. For example, for InN and GaSb, two direct-bandgap semiconductors with comparable bandgap value to VO$_2$, the bandgap narrows by 0.010 and 0.013 eV within this temperature range, respectively. This suggests that the electron correlation in VO$_2$ results in a strong bandgap renormalization upon temperature rise.

D. Thermoelectric properties

Figure 5(a) depicts the home-made setup for measuring the thermal power (Seebeck coefficient) of VO$_2$ thin film across the MIT, where the ΔT was fixed to be 1 °C for an average temperature of T. The measured Seebeck coefficient (S) is always negative, confirming the intrinsic N-type conductivity in both the insulating and metallic phases of the as-grown VO$_2$ film. The absolute values of S are shown in Fig. 5(b). The measured $|S|$ for the low-temperature insulating-phase were in the range of $400 \sim 450$ μV/°C, and in the

high temperature metallic phase, it is almost constant ($\sim$26 μV/°C), which agrees well with reported values for bulk VO$_2$ as well as single-crystal VO$_2$ nanowires.[2,21,33] From the measured S at high temperatures, it is possible to estimate the electron effective mass in the metallic phase by assuming degenerate carrier population of the band: $S = \frac{\pi^2 k^2 T}{3eE_{F0}}(3/2 + r)$,[35] where $E_{F0} = \frac{\hbar^2}{8m^*}\left(\frac{3n}{\pi}\right)^{2/3}$ is the Fermi energy at 0 K and r is the power-law index for free carrier scattering time in the Boltzmann transport theory. Using the measured electron density at 85 °C (Fig. 2(c)), we estimated m^* to be $15m_0$ and $43m_0$ by assuming a scattering index of 3/2 (ionized impurity scattering dominant) and $-1/2$ (phonon scattering dominant) respectively. Comparing these two values to the result obtained from optical reflection ($m^* \sim 23m_0$), it is found that the electron scattering in the metallic phase by phonons is insignificant.[36] This also explains the nearly temperature-independent mobility in the metallic regime in Fig. 2(d).

Within the temperature range where the metallic (M) and insulating (I) phases co-exist, the VO$_2$ film is a standard example of a dynamically changing composite system, which is of great interest for thermoelectrics due to carrier filtering at the boundaries between constituents of the composite.[37,38] We now discuss the thermoelectric and electrical properties correlatively in this temperature regime. In Fig. 5(c), we fitted the resistivity of the low-temperature I-phase (T < $\sim$60 °C) obtained from Hall measurement using the equation for non-degenerately doped semiconductors, $\rho_I(T) = \rho_{I0} \cdot \exp(E_a/k_BT)$, where the donor activation energy E_a was determined to be 0.15 eV, which is consistent with literature values of 0.13, and $0.13 \sim 0.16$ eV.[39,40] The fitted $\rho_I(T)$ was then extrapolated to high temperatures as shown in Fig. 5(c). Because of the non-one-dimensional arrangement of M/I domains in the phase co-existing regime, it is impossible to determine the I-phase fraction from overall resistance measurements. However, in a simplified "Series" model, if we assume all the M and I domains are linked in series, the effective volumetric fraction of I-phase can be estimated as $x(T) = \rho(T)/\rho_I(T)$, which is shown in Fig. 5(d). Following the work done by Cao *et al.* in 1D single-crystal VO$_2$ nano/microwires,[21] we calculated the expected effective Seebeck coefficient in the films (a 2D system in terms of domain arrangement) as a sum of contributions from the M and I domains when we neglect the contribution from the M/I domain walls, i.e.,

$$S_{expected}(T) = x(T) \times S_I(T) + \left(1 - x(T)\right) \times S_M(T), \tag{3}$$

where S_M was taken to be -26 μV/°C. $S_I(T)$ was obtained by fitting the pure I-phase below 60 °C expected from a non-degenerately doped semiconductor: $S_I(T) = (k_B/e) \cdot (5/2 + r + |E_F|/k_BT)$,[41] and then extrapolated to high temperatures. Here, $|E_F|$ is the Fermi energy measured from the bottom of the conduction band, which was determined from the fitting to be $\sim$0.17 eV below the conduction band minimum. It is noted that the position of the Fermi level relative to the bottom of the conduction band, although in disagreement with the picture obtained by ultraviolet photoemission measurements in VO$_2$ single crystals,[42] is consistent with the
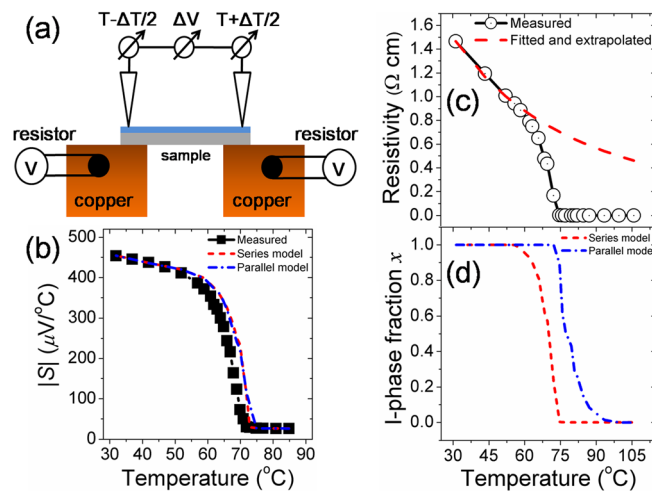

FIG. 5. Thermoelectric properties. (a) Schematic of the home-made setup for temperature-dependent thermal power measurement. (b) Seebeck coefficient of VO$_2$ thin film measured as a function of temperature. Lines are the Seebeck coefficients expected from the measured resistivity in (c) using two simplified models. (c) Hall resistivity of the VO$_2$ thin film at different temperatures. Red line is a fit of the resistivity in the pure insulating-phase and extrapolated to the high temperature metallic-phase. (d) Temperature-dependent volumetric fraction of the insulating-phase determined from resistivity in (c) in the two models.

N-type conduction of the film as identified by the Hall as well as Seebeck measurements. The existence of donor-like oxygen vacancies in our polycrystalline thin film may cause the film unintentionally N-type, which agrees with a recent photoemission spectroscopy study in VO_2 thin films.[43] By fitting to the temperature-dependent electron density at low temperatures using the Boltzmann distribution approximation, $n(T) = N_c \cdot \exp[-(E_c - E_F)/k_B T]$, where $N_c = 2\left(\frac{2\pi m^* k_B T}{h^2}\right)^{3/2}$ is the effective density of states of the conduction band. The electron effective mass in the insulating phase was determined to be $\sim 65 m_0$, which agrees well with the reported values between $60 m_0$[44] and $65 m_0$[45]. The thus-expected Seebeck coefficient from Eq. (3) is shown in Fig. 5(b) as a comparison to the measured one. If, on the other hand, we assume all the M and I domains are linked in parallel, the effective fraction of I-phase across the MIT can be estimated as $x(T) \approx 1 - \rho_M(T)/\rho(T)$, which is also shown in Fig. 5(d). It should be pointed out that we approximated $\rho_M(T)$ as a constant across the MIT. In such a purely "Parallel" model, the effective Seebeck coefficient is expected to be given by

$$\sigma(T) \cdot S_{expected}(T) = x(T) \times S_I(T) \times \sigma_I(T) + (1 - x(T)) \\ \times S_M(T) \times \sigma_M(T). \quad (4)$$

The Seebeck coefficient expected from Eq. (4) is also shown in Fig. 5(b). It can be seen that in the transition regime ($60\,^\circ C \sim 72\,^\circ C$), the measured $|S|$ is significantly lower than the expected S, by a factor of $2 \sim 3$, in both the "Series" and "Parallel" models. This discrepancy is similar to what has been observed in VO_2 nano/microwires where the metallic and insulating domains have a simpler, one-dimensionally aligned, purely series configuration.[21] This difference can be ascribed to domain wall contribution ($S_{M/I}$) to the Seebeck effect that is ignored in both the "Series" and "Parallel" models,[31] which appears to have an opposite sign and comparable value as the bulk S_I. Further experiments need to be designed and carried out to elucidate the physics of this domain wall thermoelectric effect in such a correlated electron system. For example, a simultaneously nano scale mapping of temperature and electrical potential around a single domain wall subject to a DC current flow would clarify the role of the domain wall as a junction to filter hot electrons.

IV. SUMMARY

In summary, the structural, electrical transport, optical and thermoelectric properties of high-quality epitaxial VO_2 thin films across its metal-insulator transition were systematically studied altogether. The VO_2 thin film was found to be highly oriented polycrystalline with $[010]_{M1}$ direction perpendicular to the sapphire substrate, and in-plane lattice oriented along three equivalent crystallographic directions. Across its metal-insulator transition, the variation in electron density almost entirely accounts for the change of electrical conductivity, while the electron mobility varies slightly. The electron effective mass in the metallic phase as well as the effective bandgap in the insulating phase were determined by optical reflection and absorption spectra over a wide range of temperatures. Finally, the Seebeck effect was measured as a function of temperature and discussed in correlation to the electrical transport data, pointing out to possible domain wall thermoelectric effect.

[1]Z. Yang, C. Ko, and S. Ramanathan, Annu. Rev. Mater. Res. **41**, 337 (2011).
[2]C. N. Berglund and H. J. Guggenheim, Phys. Rev. **185**, 1022(1969).
[3]A. Zylbersztejn and N. F. Mott, Phys. Rev. B **11**, 4383 (1975).
[4]R. M. Wentzcovitch, W. W. Schulz, and P. B. Allen, Phys. Rev. Lett. **72**, 3389 (1994).
[5]T. M. Rice, H. Launois, and J. P. Pouget, Phys. Rev. Lett. **73**, 3042 (1994).
[6]A. Cavalleri, T. Dekorsy, H. H. W. Chong, J. C. Kieffer, and R. W. Schoenlein, Phys. Rev. B **70**, 161102 (2004).
[7]F. J. Morin, Phys. Rev. Lett. **3**, 34 (1959).
[8]Y. J. Chang, C. H. Koo, J. S. Yang, Y.S. Kim, D. H. Kim, J. S. Lee, T. W. Noh, H.-T. Kim, and B. G. Chae, Thin Solid Films **486**, 46 (2005).
[9]T. Maruyama and Y. Ikuta, J. Mater. Sci. **28**, 5073 (1993).
[10]S. Lu, L. Hou, and F. Gan, Adv. Mater. **9**, 244 (1997).
[11]Z. Yang, C. Ko, and S. Ramanathan, J. Appl. Phys. **108**, 073708 (2010).
[12]D. H. Kim and H. S. Kwok, Appl. Phys. Lett. **65**, 3188 (1994).
[13]N. R. Mlyuka, G. A. Niklasson, and C. G. Granqvist, Appl. Phys. Lett. **95**, 171909 (2009).
[14]M. Nakano, K. Shibuya, D. Okuyama, T. Hatano, S. Ono, M. Kawasaki, Y. Iwasa, and Y. Tokura, Nature **487**, 459 (2012).
[15]B. Hu, Y. Ding, W. Chen, D. Kulkarni, Y. Shen, V. V. Tsukruk, and Z. L. Wang, Adv. Mater. **22**, 5134 (2010).
[16]J. Cao, W. Fan, Q. Zhou, E. Sheu, A. Liu, C. Barrett, and J. Wu, J. Appl. Phys. **108**, 083538 (2010).
[17]D. Ruzmetov, D. Heiman, B. B. Claflin, V. Narayanamurti, and S. Ramanathan, Phys. Rev. B **79**, 153107 (2009).
[18]M. M. Qazilbash, M. Brehm, B.-G. Chae, P.-C. Ho, G. O. Andreev, B.-J. Kim, S. J. Yun, A. V. Balatsky, M. B. Maple, F. Keilmann, H.-T. Kim, and D. N. Basov, Science **318**, 1750 (2007).
[19]Y. Gu, J. Cao, J. Wu, and L.-Q. Chen, J. Appl. Phys. **108**, 083517 (2010).
[20]R. Cabrera, E. Merced, N. Sepúlveda, and F. E. Fernández, J. Appl. Phys. **110**, 094510 (2011).
[21]J. Cao, W. Fan, H. Zheng, and J. Wu, Nano Lett. **9**, 4001 (2009).
[22]W. T. Liu, J. Cao, W. Fan, H. Zhao, M. C. Martin, J. Wu, and F. Wang, Nano Lett. **11**, 466 (2011).
[23]S. Lysenko, V. Vikhnin, F. Fernandez, A. Rua, and H. Liu, Phys. Rev. B **75**, 075109 (2007).
[24]P. Mandal, A. Speck, C. Ko, and S. Ramanathan, Opt. Lett. **36**, 1927 (2011).
[25]T.-H. Yang, R. Aggarwal, A. Gupta, H. Zhou, R. J. Narayan, and J. Narayan, J. Appl. Phys. **107**, 053514 (2010).
[26]G. J. Kovács, D. Bürger, I. Skorupa, H. Reuther, R. Heller, and H. Schmidt, J. Appl. Phys. **109**, 063708 (2011).
[27]T.-H. Yang, S. Mal, C. Jin, R. J. Narayan, and J. Narayan, Appl. Phys. Lett. **98**, 022105 (2011).
[28]K. Okimura, J. Sakai, and S. Ramanathan, J. Appl. Phys. **107**, 063503 (2010).
[29]J. Cao, E. Ertekin, V. Srinivasan, W. Fan, S. Huang, H. Zheng, J. W. L. Yim, D. R. Khanal, D. F. Ogletree, J. C. Grossman, and J. Wu, Nature Nanotech. **4**, 732 (2009).

[30]W. H. Rosevear and W. Paul, Phys. Rev. B **7**, 2109 (1973).

[31]P. Perlina, E. Litwin-Staszewska, B. Suchanek, W. Knap, J. Camassel, T. Suski, R. Piotrzkowski, I. Grzegory, S. Porowski, E. Kaminska, and J. C. Chervin, Appl. Phys. Lett. **68**, 1114 (1996).

[32]A. S. Barker, H. W. Verleur, and H. J. Guggenheim, Phys. Rev. Lett. **17**, 1286 (1966).

[33]D. H. Hensler, J. Appl. Phys. **39**, 2354 (1968).

[34]S. Sirohi and T. P. Sharma, Opt. Mater. **13**, 267 (1999).

[35]D. K. C. MacDonald, *Thermoelectricity: An Introduction to the Principles* (Dover Publications, Inc., 2006), p. 27.

[36]M. M. Qazilbash, K. S. Burch, D. Whisler, D. Shrekenhamer, B. G. Chae, H. T. Kim, and D. N. Basov, Phys. Rev. B **74**, 205118 (2006).

[37]D. Vashaee and A. Shakouri, Phys. Rev. Lett. **92**, 106103 (2004).

[38]G. Zeng, J. M. O. Zide, W. Kim, J. E. Bowers, A. C. Gossard, Z. Bian, Y. Zhang, A. Shakouri, S. L. Singer, and A. Majumdar, J. Appl. Phys. **101**, 034502 (2007).

[39]X. Wu, Y. Tao, L. Dong, Z. Wang, and Z. Hu, Mater. Res. Bull. **40**, 315 (2005).

[40]F. Guinneton, L. Sauques, J. C. Valmalette, F. Cros, and J. R. Gavarri, J. Phys. Chem. Solids **62**, 1229 (2001).

[41]J. Cai and G. D. Mahan, Phys. Rev. B **74**, 075201 (2006).

[42]S. Shin, S. Suga, M. Taniguchi, M. Fujisawa, H. Kanzaki, A. Fujimori, H. Daimon, Y. Ueda, K. Kosuge, and S. Kachi, Phys. Rev. B **41**, 4993 (1990).

[43]D. Ruzmetov, K. T. Zawilski, S. D. Senanayake, V. Narayanamurti, and S. Ramanathan, J. Phys.: Condens. Matter **20**, 465204 (2008).

[44]A. Zylberstejn, B. Pannetier, and P. Merenda, Phys. Lett. A **54**, 145 (1975).

[45]J. M. Reyes, M. Sayer, A. Mansingh, and R. Chen, Can. J. Phys. **54**, 413 (1976).